

## Modelling of Cast Iron to Carbon Electrical Contact Resistance to Reproduce Anode Voltage Measurements

Louis Bugnion<sup>1</sup>, René von Kaenel<sup>2</sup>, Roman Düssel<sup>3</sup> and André van Haaren<sup>4</sup>

1. Head of modelling

2. CEO

KAN-NAK, Switzerland

3. Plant manager

4. Process engineer

TRIMET Aluminium, Germany

Corresponding author: louis.bugnion@kannak.ch

<https://doi.org/10.71659/icsoba2024-el016>

### Abstract

Anode voltage (or anode assembly voltage) is an important component of the voltage breakdown of an electrolysis cell. It contributes to the specific energy consumption of the produced aluminium and to the cell internal heat generation required to maintain the right operating temperature and ledge protection. In general, it is beneficial to reduce the anode voltage to save energy or generate heat in the ACD rather than in the anode. High anode voltage may also reflect poor distributions of anode current density or mechanical stresses which enhance the probability of anodic incidents such as cracks and burn-offs. Nevertheless, anode voltage correlates with the anode thermal resistance which contributes to the cell top heat loss and thus reducing the anode voltage does not necessarily mean a lower cell voltage assuming the same thermal balance.

The main components of the anode voltage are the yoke and stubs voltages including the clad voltage, the stub to cast iron contact voltage, the cast iron voltage, the cast iron to carbon contact voltage and the carbon voltage. They can be easily determined numerically from temperature and current density fields knowing temperature-dependent material properties, except for the contact voltages. We assume that the cast iron to carbon contact voltage depends on the contact pressure between cast iron and carbon at operating temperature which in turn is a function of the air gap resulting from the cast iron and stub shrinkages after anode rodding. The coupled thermoelectric-mechanical problem is solved to compute the anode voltage. The law relating the contact surface resistivity and the contact pressure is calibrated based on measurements over the cycle of Reference anodes and validated based on measurements over the cycle of so-called “Big Foot” anodes having different stub and stub hole geometries. Mechanisms responsible for the anode voltage breakdown as a function of yoke, stub, stub hole, carbon block designs and anode age are highlighted. Similar models can also find application in cathode design which also involves a cast iron to carbon electrical contact.

**Keywords:** Anode voltage measurement, Cast iron to carbon electrical contact resistance, TE-MEC modelling, Stub hole design, “Big Foot” anode.

### 1. Introduction

Electrical contact between conductor surfaces is achieved by contact points which carry the electrical current and reduce the effective contact area. The electrical contact, despite a very short length, is characterized by a voltage drop which can be modelled by an electrical contact resistance. The stub to cast iron contact resistance is generally assumed to be negligible and the focus is laid on the cast iron to carbon contact (both being difficult to distinguish experimentally). In previous modelling work [1], the electrical contact resistance between cast iron and carbon is assumed to depend on the pressure between the contact surfaces. The contact pressure results

from the lifting of the anode by the anode rod and by the heating of the anode from ambient temperature to operating temperature. It depends on the anode geometry (including the air gap between cast iron and carbon consecutive to rodding), on the operating temperature and current density fields and on the material properties of the anode components (electrical and thermal conductivities, thermal expansion coefficient, Young's modulus). Thus, a coupled thermoelectrical-mechanical problem must be solved to compute the anode voltage. In practice, the cast iron to carbon electrical contact resistance of a given anode design is often calibrated based on anode voltage measurements. However, this approach loses its predictive capability in case of change of anode design or material properties.

## 2. Models

### 2.1 Reference

An existing anode assembly called hereafter the Reference anode has been modelled including: clad, yoke, stubs, cast iron, air gap, carbon block, anode cover, crust, bath and metal layers with respective material properties at three different anode ages (7, 14 and 21 days). The carbon block height as a function of anode age has been computed based on new anode and butt heights (see Figure 1). It is assumed that only the height of carbon block and crust layer is affected by anode age, the carbon block cross section being unchanged. The decrease in crust thickness with anode age is a consequence of the assumed constant anode cover thickness.

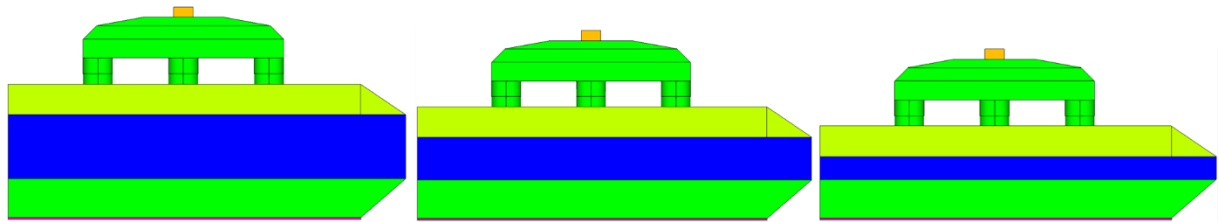


Figure 1. Reference anode assembly model: 7, 14 and 21 days.

The air gap between cast iron and carbon at ambient temperature results from the shrinkage of cast iron and stubs after rodding and from the downward movement of the carbon block when the anode is lifted (due to the air gap on the flutes sides, carbon block is supported by the upper flutes side). The air gap is not uniform across the contact surfaces due to the varying cast iron thickness and flute width over the stub hole depth. The air gap between the flutes and at the flute tip is the sum of the cast iron and stub shrinkages as expressed in Equation 1.

$$\begin{aligned} \text{gap} &= \Delta r_{\text{stub}} + \Delta d_{\text{cast-iron}} \\ &= r_{\text{stub}} \cdot \alpha_{\text{steel}} \cdot (T_{\text{stub}} - T_{\text{amb}}) + d_{\text{cast-iron}} \cdot \alpha_{\text{cast-iron}} \cdot (T_{\text{cast-iron-solid}} - T_{\text{amb}}) \end{aligned} \quad (1)$$

where:

$r_{\text{stub}}$	Stub radius, m
$d_{\text{cast-iron}}$	Cast iron distance, m
$\alpha_{\text{steel}}, \alpha_{\text{cast-iron}}$	Thermal expansion coefficients, °C <sup>-1</sup>
$T_{\text{stub}}$	Stub temperature before rodding, °C
$T_{\text{cast-iron-solid}}$	Cast iron solidification temperature, °C
$T_{\text{amb}}$	Ambient temperature, °C

On the flute sides, the air gap is only made by the shrinkage of cast iron  $\Delta d_{\text{cast-iron}}$  with  $d_{\text{cast-iron}}$  being the flute width. In contrast to [1], the contact pressure is also computed below the stubs and current is allowed to flow from stub end to carbon assuming the same contact resistance as between cast iron and carbon.

Boundary conditions are constant bath and metal temperatures and clad temperature depending on anode age based on measurements shown in Figure 2. Thermal convection is applied to the model components in contact with air by using a heat transfer coefficient. Electrical current is injected at the clad top surface and zero electrical potential is applied at the metal layer bottom surface.

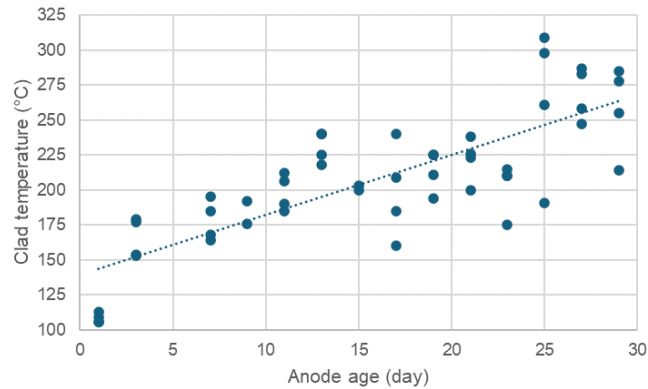


**Figure 2. Measured clad temperature as a function of anode age**

## 2.2 Big Foot

So-called Big Foot anodes have been tested at TRIMET Essen smelter. They consist in anodes with modified stub and stub hole designs. Stub diameter is enlarged in the lower half of the stub hole and cast-iron thickness is slightly increased around the enlarged stub to maintain the mechanical stress in the stub hole at an acceptable level. Cast iron is poured only in the lower half of the stub hole. A thin horizontal groove is machined around the stub hole at the top of the enlarged stub and is filled by cast iron during rodding. The Big Foot design suppresses the cast iron flutes whose electrical contact to carbon is poorer than between the flutes. The contact surface between cast iron and carbon is smaller compared to the reference (-20 %) but the contact surface in the upper half of the stub hole which yields low contact pressure (due to lower stub temperature and larger cast iron thickness) is gotten rid of. Stub diameter is enlarged only in the lower half of the stub hole to limit cast iron demand and top heat loss. The air gap is modelled according to Equation 1. The downward movement of the carbon block when the anode is lifted is due to the cast iron shrinkage in the groove. Same boundary conditions are applied as for the Reference anode.

## 3. Results

The three Reference and three Big Foot anode models have been computed using a finite-element method. The contact surface resistivity between cast iron and carbon has been assumed to follow an exponential law with respect to contact pressure whose parameters have been calibrated to reproduce the measured min-max anode voltage values of Reference anodes (see Figure 3). During the trial, min-max anode voltage (voltage from clad to bottom outer corner of carbon block) and anode current of three Reference anodes and three Big Foot anodes have been measured daily to determine the min-max anode resistance over an anode cycle. In Figure 4, measured average min-max anode resistance values multiplied by the average anode current are plotted versus anode age along with the corresponding values computed for the Reference and Big Foot anode models (at 7, 14 and 21 days). The same exponential law has been used for the Big Foot anode models. Measured min-max voltage values are 65 mV higher at 7 days (computed 55 mV higher) and 50 mV higher at 21 days (computed 45 mV higher) for Reference anodes

compared to Big Foot anodes. These figures are discussed in more detail when analysing the effective anode voltage breakdown. It seems that the model underestimates the decrease in voltage over the anode cycle as well as the difference in voltage between Reference and Big Foot anodes. One possible reason is that the clad temperature as a function of anode age was not measured during the trial but later on, only for Reference anodes, and was assumed to be the same for Big Foot anodes. Additional modelling could help at refining this assumption.

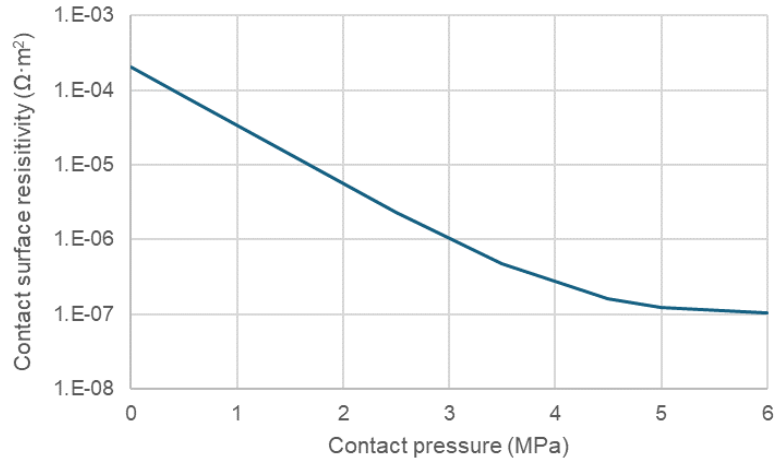


**Figure 3. Calibrated exponential law relating contact surface resistivity to contact pressure.**

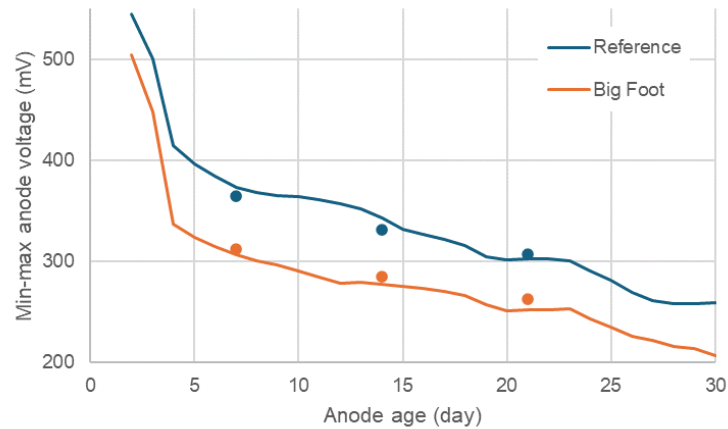


**Figure 4. Measured average min-max anode voltage (normalized to average anode current) versus anode age along with computed min-max anode voltage values at 7, 14 and 21 days for Reference and Big Foot anodes.**

Figures 5, 6 and 7 show computed cast iron to carbon contact temperature, normal stresses and current density fields for Reference and Big Foot anodes at 7 days. Computed temperature shows lower values in the middle stub (lower thermal resistance compared to inner and outer stubs) and for the Reference anode. Temperature increases from stub hole bottom to stub hole top by 90 °C for the Reference anode and by only 30 °C for the Big Foot anode. This shows that the thermal expansion of carbon, cast iron and stubs is not uniform over the stub hole depth.

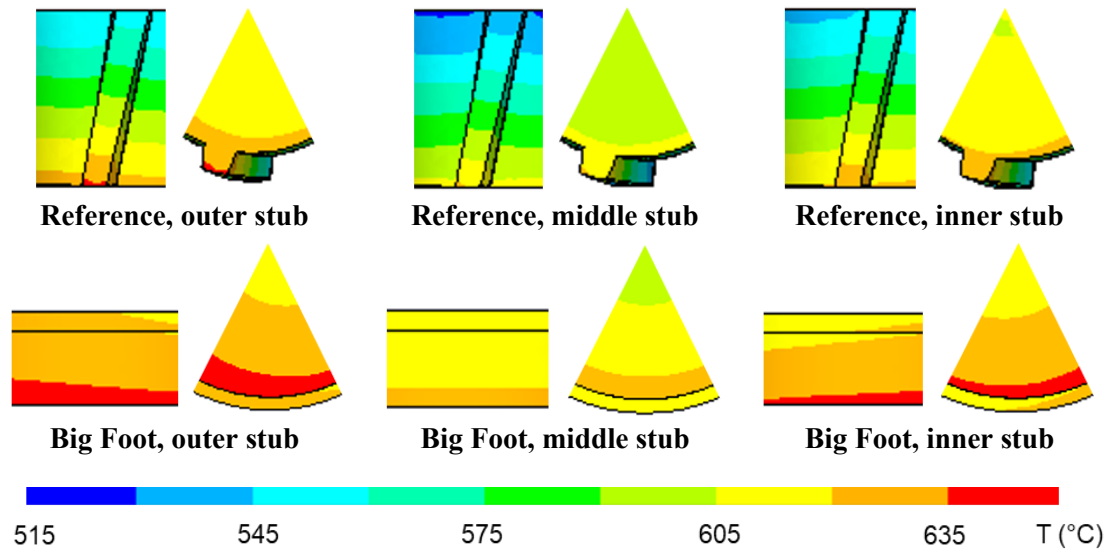


Figure 5. Computed cast iron to carbon contact temperature at 7 days for Reference and Big Foot anodes.

Computed normal stresses also vary over the stub hole depth. Between the flutes,  $\sigma_{xx}$  decreases from 10 MPa (negative sign indicates compression) at the bottom to 2 MPa at the top. This is a result of decreasing temperature towards the top and of increasing air gap thickness due to the flared stub hole geometry. At the flute tip, the trend is similar but  $\sigma_{xx}$  is lower due to the larger air gap (thicker cast iron). On the stubs side, normal stresses are larger for the Big Foot anode compared to the Reference anode. Below the stubs, the stub thermal expansion compensates for the downward movement of the carbon block resulting in low compressive stress ranging from 0 to 4 MPa. The flutes upper side experiences similar low compressive stress due to the carbon block weight whereas there is almost no contact on the flutes lower side (positive normal stress).

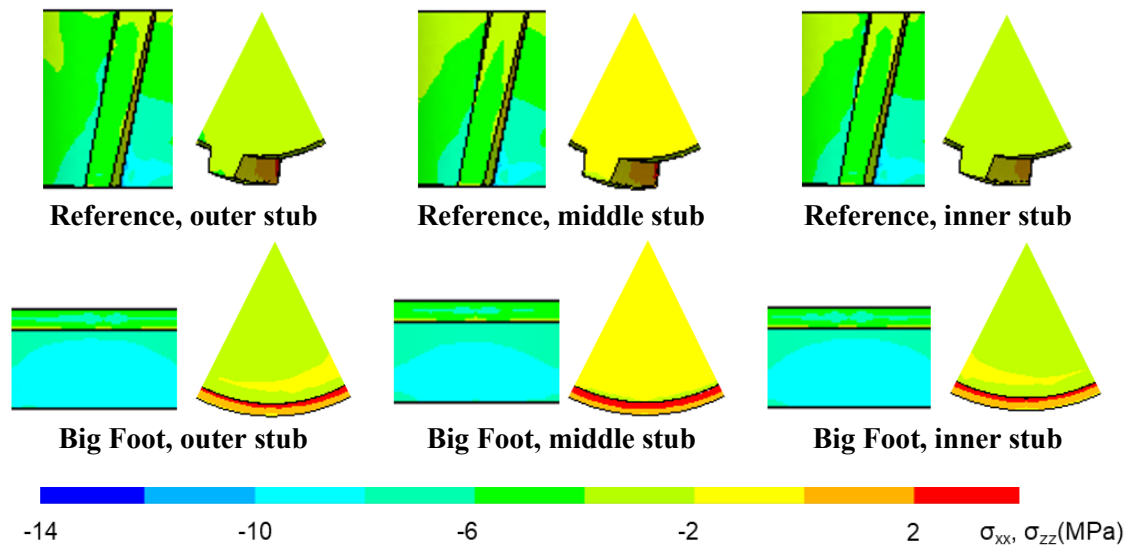
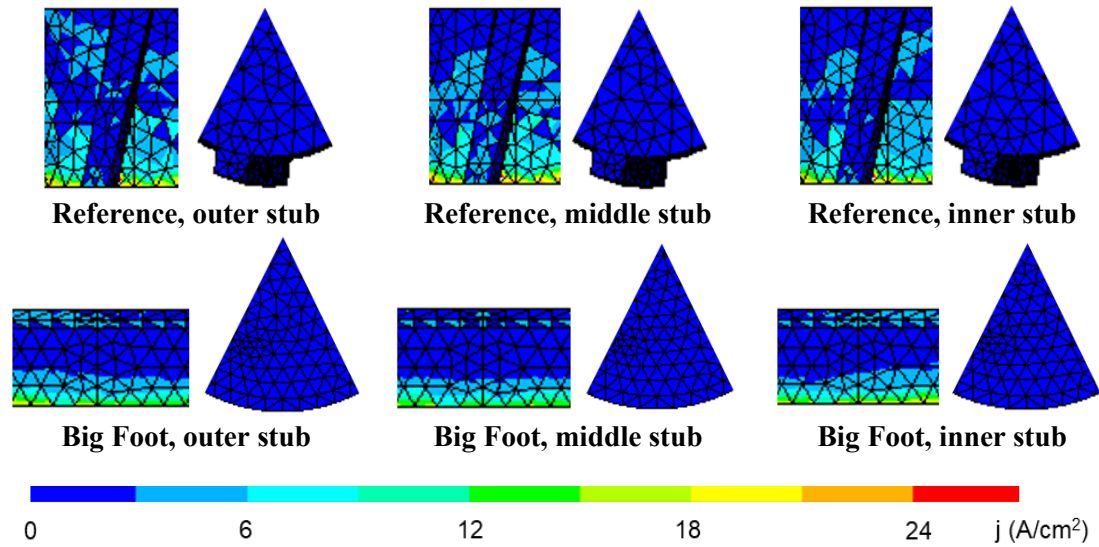


Figure 6. Computed cast iron to carbon contact normal stresses ( $\sigma_{xx}$  on the side and  $\sigma_{zz}$  on the bottom) at 7 days for Reference and Big Foot anodes.

For the Reference anode, current density is maximum between the flutes at the bottom of the stub hole. Current is flowing at the flute tip but to a lesser extent and mainly close to the bottom of the stub hole. Only little current is flowing below the stubs. For the Big Foot anode, current density

is also larger close to the stub hole bottom and is not interrupted by the flutes. However, maximum current density values are lower which reflects positively on the voltage.



**Figure 7. Computed cast iron to carbon contact current density at 7 days for Reference and Big Foot anodes.**

Current density and temperature fields together with material and contact properties determine the voltage drop over the anode assembly. In the following, we consider the effective voltage drop which is computed as the Ohmic power in each anode component divided by anode current (effective voltage is more relevant than the min-max voltage since it relates to the energy consumption, however it cannot be measured except if it coincides with the min-max voltage). The effective anode voltage breakdown is represented in Figure 8 and Table 1 for the Reference and Big Foot anodes. Clad, yoke and cast-iron voltages are similar for Reference and Big Foot anodes and increase slightly with anode age due to higher temperature. Cast iron to carbon contact voltages are larger for the Reference anode compared to the Big Foot anode despite larger contact surfaces. This is a result of higher contact pressure leading to lower electrical contact resistance. Nevertheless, contact voltages for the Reference anode are in the lower range compared to other technologies. Contact voltages of the Big Foot anode are less sensitive to anode age since contact pressure remains in a range where contact surface resistivity varies little. The carbon voltage decreases with anode age as a result of lower carbon height, higher carbon temperature and more uniform current density around the stub hole (due to higher contact pressure). Interestingly, the anode voltage saving at 7 days for the Big Foot anode is more than twice larger in the carbon than in the cast iron to carbon contact.

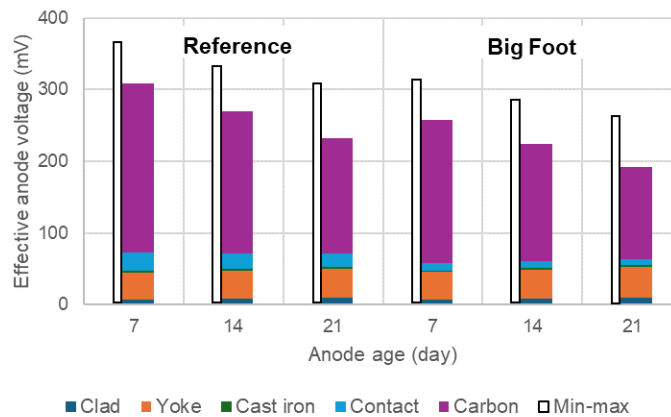


**Figure 8. Computed min-max anode voltage and effective anode voltage breakdown at 7, 14 and 21 days for Reference and Big Foot anodes.**

**Table 1. Computed min-max anode voltages and effective anode voltage breakdown at 7, 14 and 21 days for Reference and Big Foot anodes.**

	Anode age day	Min-max mV	Effective mV	Clad mV	Yoke mV	Cast iron mV	Contact mV	Carbon mV
<b>Reference</b>	7	365	309	7	37	3	25	237
	14	331	269	8	39	3	22	198
	21	307	232	9	41	3	19	161
<b>Big Foot</b>	7	312	258	7	38	2	10	200
	14	285	224	8	40	2	10	163
	21	263	191	9	43	2	9	127

#### 4. Conclusions

A model for the electrical contact resistance between cast iron and carbon is proposed and calibrated based on anode voltage measurements by solving the thermoelectric-mechanical problem of an anode immersed in bath and conducting electrical current to a metal layer. The model has been validated by computing an alternative anode design which was tested at TRIMET Essen smelter. The computation results highlight the mechanisms responsible for the variations in anode voltage breakdown as a function of anode design and age.

Based on our experience of Hall-Héroult cell technologies, cast iron to carbon contact voltage ranges from 20 mV as for the Reference anode to up to 100 mV depending on anodic current density and anode design. As demonstrated with the Big Foot anode, the voltage drop over the cast iron to carbon contact can be reduced by stub and/or stub hole design changes but the voltage drop in the carbon block can be decreased to an even larger extent if the current density around the stub hole is made more uniform. Heat loss through the yoke and the anode cover has not been studied here but should be part of the full analysis to make sure that the anode voltage saving can be recovered in the cell voltage.

#### 5. References

1. Daniel Richard et al., Challenges in stub hole optimisation of cast iron rodded anodes, *Light Metals*, 2009, 1067–1072.